(12) INTERNATIONAL APPLICATION PUBLISHED UNDER THE PATENT COOPERATION TREATY (PCT)

(19) World Intellectual Property Organization
International Bureau

(43) International Publication Date
03 September 2026 (03.09.2026)

WIPO | PCT

(10) International Publication Number
WO 2026/183497 A1

(51) International Patent Classification:
G02F 1/139 (2006.01) *C08J 3/28* (2006.01)
G02B 5/30 (2006.01) *C09K 19/52* (2006.01)
G02F 1/1334 (2006.01)

(21) International Application Number:
PCT/US2026/017119

(22) International Filing Date:
27 February 2026 (27.02.2026)

(25) Filing Language: English

(26) Publication Language: English

(30) Priority Data:
63/764,363 27 February 2025 (27.02.2025) US

(71) Applicant: **THE REGENTS OF THE UNIVERSITY OF COLORADO, A BODY CORPORATE** [US/US]; 1800 Grant Street, 8th Floor, Denver, CO 80203 (US).

(72) Inventors: **SMALYUKH, Ivan, I.**; 1465 Ithaca Drive, Boulder, CO 80305 (US). **ZHAO, Hanqing**; 2040 Athens Street, Apartment E, Boulder, CO 80308 (US).

(74) Agent: **PILLOTE, Cynthia, L.**; Snell & Wilmer L.l.p., 1 East Washington Street, Suite 2700, Phoenix, AZ 85004-2556 (US).

(81) Designated States *(unless otherwise indicated, for every kind of national protection available)*: AE, AG, AL, AM, AO, AT, AU, AZ, BA, BB, BG, BH, BN, BR, BW, BY, BZ, CA, CH, CL, CN, CO, CR, CU, CV, CZ, DE, DJ, DK, DM, DO, DZ, EC, EE, EG, ES, FI, GB, GD, GE, GH, GM, GT, HN, HR, HU, ID, IL, IN, IQ, IR, IS, IT, JM, JO, JP, KE, KG, KH, KN, KP, KR, KW, KZ, LA, LC, LK, LR, LS, LU, LY, MA, MD, MG, MK, MN, MU, MW, MX, MY, MZ, NA, NG, NI, NO, NZ, OM, PA, PE, PG, PH, PL, PT, QA, RO, RS, RU, RW, SA, SC, SD, SE, SG, SK, SL, ST, SV, SY, TH, TJ, TM, TN, TR, TT, TZ, UA, UG, US, UY, UZ, VC, VN, WS, ZA, ZM, ZW.

(84) Designated States *(unless otherwise indicated, for every kind of regional protection available)*: ARIPO (BW, CV, GH, GM, KE, LR, LS, MU, MW, MZ, NA, RW, SC, SD, SL, ST, SZ, TZ, UG, ZM, ZW), Eurasian (AM, AZ, BY, KG, KZ, RU, TJ, TM), European (AL, AT, BE, BG, CH, CY, CZ, DE, DK, EE, ES, FI, FR, GB, GR, HR, HU, IE, IS,

(54) Title: CONTINUOUS SPACE-TIME CRYSTAL DEVICE AND METHOD OF FORMING AND USING SAME

FIG. 15

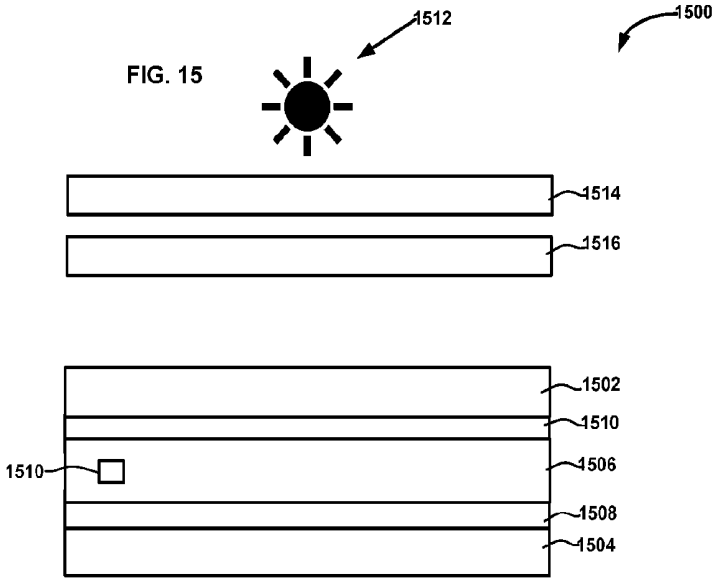

(57) **Abstract:** Continuous space-time crystal devices and methods of forming and using the devices are disclosed. Exemplary devices include a first substrate, a second substrate, a photo- responsive dye layer and/or anisotropic particles, and a nematic liquid crystal material between the first substrate and the second substrate, wherein, in response to an applied light, a continuous space-time crystallization phase forms within the nematic liquid crystal material.

WO 2026/183497 A1

[Continued on next page]

IT, LT, LU, LV, MC, ME, MK, MT, NL, NO, PL, PT, RO, RS, SE, SI, SK, SM, TR), OAPI (BF, BJ, CF, CG, CI, CM, GA, GN, GQ, GW, KM, ML, MR, NE, SN, TD, TG).

Published:

— *with international search report (Art. 21(3))*

CONTINUOUS SPACE-TIME CRYSTAL DEVICE AND METHOD OF FORMING AND USING SAME

CROSS-REFERENCE TO RELATED APPLICATIONS

[0001] This application claims the benefit of U.S. Provisional Application No. 63/764,363, entitled CONTINUOUS SPACE-TIME CRYSTAL DEVICE AND METHOD OF FORMING AND USING SAME and filed February 27, 2025, the contents of which are hereby incorporated herein by reference to the extent such contents do not conflict with the present disclosure.

STATEMENT REGARDING FEDERALLY SPONSORED RESEARCH OR DEVELOPMENT

[0002] This invention was made with government support under grant number DE-SC0019293, awarded by the U.S. Department of Energy. The government has certain rights in the invention.

FIELD OF INVENTION

[0003] The present disclosure generally relates to electronic devices. More particularly, examples of the disclosure relate to devices that exhibit continuous space-time properties.

BACKGROUND OF THE DISCLOSURE

[0004] Time crystals are recently discovered unexpected states of quantum matter that spontaneously break time translation symmetry either in a discrete or continuous manner. However, spatially-mesoscale classical space-time crystals that continuously break both the space and time symmetries have not been observed.

[0005] Fundamentally interesting properties of crystals and liquid crystals (LCs) have been driving major scientific discoveries and technological innovation for centuries. Time crystals, proposed only a decade ago, have recently captured the fascination of numerous researchers who are now contributing to this explosively growing field, although the initial concept of time crystals was shown to be unachievable—demonstrated through a series of no-go theorems proving that nature prohibits their realization in conserved systems. Differing from designs of time crystals based on closed quantum and classical many-body systems, time crystals with external Floquet drives that break time translation symmetry discretely, dubbed "discrete (Floquet) time crystals," have been demonstrated. The quantum discrete time

crystals have been observed in systems of nuclear spins, trapped ions, cold atoms, superconducting qubits and so on. Recently, a continuous time crystal has been observed in a quantum system of atom cavity, breaking the time translation symmetry continuously, which is closer to the original idea and opens a new avenue for the studies of time crystals. The continuous time crystals, differing from previously well-studied periodic open systems, should meet two stringent requirements: the order is robust against temporal perturbations (rigidity) and the relative time phase is independent of the external source (spontaneous time symmetry breaking). Continuous time crystals have also been observed in photonic meta materials, an optically pumped atomic system, Rydberg gas and an electron-nuclear spin system. However, continuous space-time crystals (CSTCs), which break the time translation symmetry as well as the space translation symmetry, have not been observed and verified yet in either quantum or classical systems. Moreover, since most of the time crystals known so far exist in the quantum world, a time crystal has not been directly seen by microscopic observations or even with bare human eyes.

[0006] Any discussion of problems and solutions set forth in this section has been included in this disclosure solely for the purpose of providing a context for the present disclosure and should not be taken as an admission that any or all of the discussion was known at the time the invention was made.

SUMMARY OF THE DISCLOSURE

[0007] Various embodiments of the present disclosure relate to classical continuous space-time crystals (CSTCs) in nematic LC systems. By shining ambient or microscope illumination light on specially designed samples with liquid crystal confined between glass plates coated by photo-responsive dye, emergent spatiotemporal patterns in which spatial and temporal symmetries are broken continuously are found. In accordance with examples of the disclosure, such emergent behavior can be directly observed in an optical microscope and even by bare eyes. In accordance with further examples, the continuous space-time crystallization phase is stable at room temperature and can survive locally for hours.

[0008] As set forth in more detail below, CSTCs may have significant fundamental implications in optical devices, photonic time crystal generators, telecommunications, anti-counterfeiting designs, and cryptography. For example, the electrical-free, light-driven, and non-contact properties of CSTCs make them especially suitable for anti-counterfeiting

applications across multiple levels. CSTCs can be used as 'time watermarks,' unique 'time fingerprints,' and 2 + 1D barcodes. Additionally, CSTCs can spatially and temporally modulate telecommunication light signals.

[0009] Embodiments of the disclosure relate to devices that exhibit continuous space-time crystal behavior. Exemplary devices include a first substrate, a second substrate, a photo-responsive dye layer, and a nematic liquid crystal material between the first substrate and the second substrate, wherein, in response to an applied light, a continuous space-time crystallization phase forms within the nematic liquid crystal material. In accordance with examples of the disclosure, the nematic liquid crystal material comprises one or more of 5CB(4-Cyano-4'-pentylbiphenyl) or E7 (a mixture of 4-Cyano-4'-pentylbiphenyl, 4'-Heptyl-4-biphenylcarbonitrile, 4'-Octyloxy-4-biphenylcarbonitrile and 4-Cyano-4'-Pentylterphenyl).

[0010] In accordance with further examples, the photo-responsive dye layer is coated onto an inner surface of one or more of the first substrate or the second substrate. The photo-responsive dye layer can be or include an azo compound, such as azobenzene or 2-(4-dimethylamino-phenylazo)-N-(3-triethoxysilane-propyl)-benzamide (dMR). In accordance with examples of the disclosure, the photo-responsive dye layer is sensitive to certain (e.g., visible) wavelengths and insensitive to other (e.g., visible) wavelengths of light. The applied light can be or include ambient light, light from a light source, and/or a polarized light source. Exemplary devices can exhibit 1 + 1D continuous space-time crystal behavior, 0 + 1D continuous space-time crystal behavior, 2 + 1D continuous space-time crystal behavior, 3 + 1D continuous space-time crystal behavior.

[0011] In accordance with additional embodiments of the disclosure, a continuous space-time crystal device includes a first substrate, a second substrate, a nematic liquid crystal material between the first substrate and the second substrate, the nematic liquid crystal material comprising anisotropic particles, and a photo-responsive dye layer coated onto one or more of the first substrate and the second substrate. As above, such devices can exhibit 1 + 1D continuous space-time crystal behavior, 0 + 1D continuous space-time crystal behavior, 2 + 1D continuous space-time crystal behavior, 3 + 1D continuous space-time crystal behavior.

[0012] Various devices described herein can include other elements. For example, exemplary devices can include other features, such as features and elements described in the appendix.

[0013] In accordance with yet additional embodiments, a telecommunications device includes a device as described herein.

[0014] In accordance with yet additional embodiments, a cryptography device includes a device as described herein.

[0015] In accordance with yet additional embodiments, an optical device includes a device as described herein.

[0016] In accordance with yet additional embodiments, a photonic time crystal generator includes a device as described herein.

[0017] In accordance with yet additional embodiments, an anti-counterfeiting system includes a device as described herein.

[0018] In accordance with yet additional embodiments, a barcode device includes a device as described herein.

[0019] These and other embodiments will become readily apparent to those skilled in the art from the following detailed description of certain embodiments having reference to the attached figures; the invention not being limited to any particular embodiment(s) disclosed.

BRIEF DESCRIPTION OF THE DRAWING FIGURES

[0020] The patent or application file contains at least one drawing executed in color. Copies of this patent or patent application publication with color drawing(s) will be provided by the Office upon request and payment of the necessary fee.

[0021] A more complete understanding of exemplary embodiments of the present disclosure can be derived by referring to the detailed description and claims when considered in connection with the following illustrative figures.

[0022] FIG. 1 illustrates (a) Schematic of a used optical microscope: the linearly polarized light passes through the LC glass cell, where the inner surfaces of substrates are coated with photo-responsive dye. The light signals and spatial patterns can be recorded by a camera after passing through the first-order retardation plate and an analyzer. (b) Schematic of an empty cell with normally incident linearly polarized blue light passing through. The dye molecules (grey cuboids) have long axes perpendicular to the polarization of the linearly polarized light. The electric field (E_x,E_y) of driving light at different depths is

shown on the right. (c) Chemical structures of the azobenzene dye and LC molecules. The LC molecule is represented as a green cylinder and the azobenzene group is shown as a grey cuboid. (d) Schematic of a LC-filled sample, where LC molecules are colored according to azimuthal angles of the director orientation, as defined by the bottom colored scheme. The electric field (E_x,E_y) of driving light at different depths of the marked areas is plotted on the right and left, respectively. (e) Experimental polarizing optical micrograph of the CSTC obtained with a first-order full-wave retardation plate. The plate's slow axis is labelled by the green double arrow and crossed polarizers are labelled by black double arrows. (f) Space-time image of the CSTC shown in (e), where the crystal size is 400μm·120s. The selected area is marked in (e); time interval is 0.3s. White scale bars indicate 50 μm in (e),(f) and yellow scale bar indicates 5s in (f). (g) Normalized red light signals extracted from space-time plot, where the selected area is marked in (f). a. u., arbitrary units. (h) Normalized Fast Fourier Transform spectrum of the light signals from (g), $\Phi(t)\rightarrow\Phi(\omega)$; the central peak is at 0.217 Hz.

[0023] FIG. 2 illustrates (a) Director field **n**(**r**) of a CSTC in *x*-*y* (top) and *x*-*z* (bottom) cross-sections. **n**(**r**) is translationally invariant along the *y* axis, as illustrated *x*-*y* cross-section at the bottom surface. Light propagation directions are from *z* to -*z*; the cylinders are colored according to the circle scheme on the right. (b) Along the spatial paths γ_1 and γ_2 marked in (a), the director **n** rotates by +π and -π, respectively. Since $\mathbb{S}^1/\mathbb{Z}_2 \cong \mathbb{S}^1$, the mappings of director orientations from these paths cover the order parameter space once in opposite directions, indicating the +1 and -1 Néel domain wall solitons at region I and II in (a). (c) Elastic free energy density in the *x*-*z* cross-section marked in (a). The free energy density is calculated using Eq. (1) and relative to that of a uniform nematic background. It is visualized using grayscale scheme (right-side inset); a.u., arbitrary units. (d) Schematic of many-body interactions among the topological solitonic quasiparticles at different times, where *T* is the temporal periodicity of the CSTC. (e),(f) Probability distributions of displacements of neighboring domain wall solitons (e) and corresponding potential landscape (f); inset shows measurements of displacements, where *L* is the spatial periodicity. (g),(h) Simulated polarizing optical micrograph snapshot (g) and space-time image (h) of the CSTC. The selected area (h) is marked in (g). (i) Experimental measured temporal periodicity as a function of the temperature and driving light intensity. (j) Simulated temporal periodicity versus temperature and light coupling efficiency; temporal periodicities T are colored according to the schemes in right-side insets, whereas regions of disorder and TSU phases are shown in grey.

[0024] FIG. 3 illustrates (a) Space-time image shows that the CSTC order recovers from an emergence of space-time dislocation, with the stripe pattern's slope of $\tan^{-1} L/T$. (b) Layer displacement profile prediction (red solid lines) fits the experimental results (blue dots) reconstructed from (a). The horizontal coordinates are derived from the spatial coordinate x minus tL/T. (c) Space-time image of the CSTC under temporal perturbations. White scale bar is 10 μm and yellow scale bar is 3 s. The retardation plate's slow axis is labelled by the green double arrow and crossed polarizers are labelled by black double arrows. (d) Normalized light signals Φ(t) when temporally randomizing the driving light intensity. The time interval for each random step is 0.1s. a. u., arbitrary units. (e) A simulated realization obtained after temporally randomizing the light coupling efficiency. The time interval for each random step is 0.01s. (f) Experiment measured crystal fraction $\Xi=\sum_{1/T-\delta}^{1/T+\delta}\Phi(\omega/2\pi)$ versus α, the driving light intensity is randomly distributed in $[\alpha,1]W_{driving}$, where $W_{driving}$=1.5 mWcm^{-2} and δ=0.03Hz. (g) Normalized light signals Φ(t) for α=1 (top) and α=0.4 (bottom). (h) Computer simulated $\Xi=\sum_{1/T-\delta}^{1/T+\delta}n_x(\omega/2\pi)$ versus α, with the light coupling efficiency randomly distributed in $[\alpha,1]\eta_{max}$, where η_{max}=0.5 and δ=0.03Hz. (i) Simulations for α=1 (top) and α=0.4 (bottom).

[0025] FIG. 4 illustrates (a) Space-time image of an experimental realization to measure the relative time phase. We first block the driving light with a red color filter, then calculate the relative time phase with the light signal sequence Φ(t) after a time interval Δt. White scale bar is 10 μm and yellow scale bar is 3 s. The retardation plate's slow axis is labelled by the green double arrow and crossed polarizers are shown by black double arrows. (b) Two experimental realizations, which have a time phase difference about π. a. u., arbitrary units. (c) Experimentally measured distribution of the relative time phases. (d) A simulated realization that shows the evolution of x component of the director after blocking-unblocking the external drive. (e) Simulated distribution of relative time phases calculated while using the x component of **n**(**r**).

[0026] FIG. 5 illustrates (a) Schematic of the phase accumulation process when the blue driving light (450nm, shown by blue arrows) passes through the cell. (b) Spatial and temporal distribution of the output light polarizations within one temporal (T) and spatial (L) period, as the 450 nm linearly-polarized input driving light passes through the cell. (c) Schematic of the phase accumulation process when the modulated light (1300 nm, shown by red arrows) passes through the cell. Linear and elliptical polarization states of the light in (a)

and (c) are marked by the black double arrows and ellipses, respectively. Cylinder colors represent azimuthal angles of **n**(**r**) orientation defined by the scheme in the right inset of (a). (d) Spatial and temporal distribution of the output light polarizations within one *T* and *L* periods, as the 1300 nm linearly-polarized input modulated light passes through the cell. In (b) and (d), left- and right-handed elliptical polarization states are marked by blue and red arrows, respectively.

[0027] FIG. 6 illustrates (a)-(c) Polarizing optical micrographs of disordered states (a),(b) and the CSTC of spatiotemporal topological solitons (c) that can serve as a "time watermark". (d) Two spontaneously formed experimental fingerprint states assembled from multiple CSTCs. (e) Another pair of spontaneously formed numerically simulated fingerprint states assembled from multiple CSTCs. These fingerprint states are non-identical and the vertical axis in (d),(e) represents individual CSTCs. (f) By smoothly changing the light coupling efficiency (top) in different realizations (plot with blue and red, respectively), the CSTC phase, shown by the evolution of x component of **n**(**r**), can be tuned to any desired angle (bottom); the phase difference depends on the tuning process. (g) A snapshot of a 2 + 1D barcode created by superimposing two fingerprint states, displayed by grayscale. Using the phase tuning method, information can be encoded and stored in this 2 + 1D barcode. (h) Polarizing optical micrographs of two CSTCs, captured over time. The temporal periodicity of top row CSTC is 3.48 s while that of the bottom row is 4.54 s. Thus, after ~15 s (14.90 s), the phase of top CSTC aligns with that of the bottom one. (i) Fingerprint states assembled from numerically simulated CSTCs over a 10 s interval, with each row's CSTC having a different *T*. The right state cannot be generated by shifting the left fingerprint state by the same phase angle. However, if the temporal periodicity of CSTCs in each row is known, the right state can be predicted from the left fingerprint state.

[0028] FIG. 7 illustrates space-time image of a CSTC obtained for the cell thickness *d* = 4 μm. White scale bar indicates 50 μm; yellow scale bar indicates 10 s. The retardation plate's slow axis is labelled by the green double arrow and crossed polarizers by black double arrows.

[0029] FIG. 8 illustrates correlation function *G*(t) versus time. The red solid line is the fit of power law decay, with an exponent of -0.09, indicating quasi-long-range order in time.

[0030] FIG. 9 illustrates (a) Director field **n**(r) in the *x*-*z* cross-section that has a small perturbation on the left side. The structure is invariant along the *y* direction. (b)-(d) Simulated

director field **n**(**r**) shows the spontaneous emergence of spatially periodic structures stemming from a small perturbation starting from (a). The cylinder colors represent azimuthal angles of the director orientation as defined by the colored circle in the bottom right of (a). The elapsed times are marked on their top and the light propagation directions are marked on their right, respectively. (e)-(h) Simulated polarizing optical micrographs corresponding to the structures of director field of (a)-(d), respectively. The retardation plate's slow axes are labelled by green double arrows and crossed polarizers by black double arrows.

[0031] FIG. 10 illustrates (a),(b), Experimental (a) and numerically simulated (b) polarizing optical micrographs of CSTCs. The slow axes of a phase retardation plate are labelled by green double arrows and crossed polarizers by black double arrows. (c),(d) Experimental (c) and numerically simulated (d) three-photon excitation fluorescence polarizing microscopy images obtained for different linearly polarized femtosecond laser excitations, with marked excitation light polarizations (blue double arrows). White scale bars indicate 5 μm.

[0032] FIG. 11 illustrates (a) An orthorhombic lattice pattern generated by orthogonally superimposing polarizing optical micrograph snapshots of two CSTCs. (b) An orthorhombic lattice pattern derived from space-time images of two CSTCs, where the selected area is marked in (a) with dashed rectangles. (c) A monoclinic lattice pattern generated by obliquely superimposing polarizing optical micrograph snapshots of two CSTCs. (d) A monoclinic lattice pattern produced from space-time images of two CSTCs, where the selected area is marked in (c) with dashed rectangles. The 2×2 white lattices in (b) and (d) correspond to the orthorhombic and monoclinic lattices, respectively. Spatial and temporal axes are labelled in each image.

[0033] FIG. 12 illustrates Space-time images of CSTCs with different temporal periodicity driven by the low (top) and high (bottom) intensity, respectively. White scale bars indicate 20 μm and yellow scale bars indicate 10 s; the crossed polarizers are labelled by black double arrows.

[0034] FIG. 13 illustrates (a) Simulated director field of the TSU phase. The structure is invariant along the *y* direction, and the illustrated *x*-*y* cross-section of director field is at the mid-plane along *z* direction of the sample. The polarization of the linearly polarized light is along *y* direction at the top surface, and the propagation direction is marked on the right. The cylinders are colored based on the azimuthal angles of the director, as defined by the colored

circle on the bottom right. (b),(c) Experimental (b) and numerically simulated (c) polarizing optical micrographs of the TSU phase. White scale bar indicates 20 μm; the slow axes of a phase retardation plate are labelled by green double arrows and crossed polarizers by black double arrows.

[0035] FIG. 14 illustrates the CSTC area shows a good spatial and temporal periodicity, which appears from the emerging area. White scale bar indicates 50 μm. The slow axis of a phase retardation plate is labelled by the green double arrow; crossed polarizers by black double arrows.

[0036] FIG. 15 illustrates a device in accordance with examples of the disclosure.

DETAILED DESCRIPTION OF EXEMPLARY EMBODIMENTS

[0037] Although certain embodiments and examples are disclosed below and in the attached materials, it will be understood by those in the art that the invention extends beyond the specifically disclosed embodiments and/or uses of the invention and obvious modifications and equivalents thereof. Thus, it is intended that the scope of the invention disclosed should not be limited by the particular disclosed embodiments described below.

[0038] In this disclosure, any two numbers of a variable can constitute a workable range of the variable, and any ranges indicated may include or exclude the endpoints. Additionally, any values of variables indicated (regardless of whether they are indicated with about or not) may refer to precise values or approximate values and include equivalents, and may refer to average, median, representative, majority, or the like, in some embodiments. For example, the term about can refer to +/- 20, 10, 5, 2, or 1 percent of a value. Further, in this disclosure, the terms including, comprising, constituted by and having and their equivalents can refer independently to typically or broadly comprising, consisting essentially of, or consisting of in some embodiments. In accordance with aspects of the disclosure, any defined meanings of terms do not necessarily exclude ordinary and customary meanings of the terms.

[0039] As set forth in more detail below, various examples of the disclosure relate to devices that include a continuous space-time crystal in a nematic liquid crystal. Exemplary devices described herein can be driven by shining (e.g., ambient) power, (e.g., constant)-intensity (e.g., unstructured) light. A space-time crystallization phase, as described herein,

can be formed by particle-like topological solitons. Robustness against temporal perturbations and spatiotemporal dislocations shows the stability and rigidity of the space-time crystals, which relates to their locally topological nature and many-body interactions between emergent spontaneously-twisted, particle-like solitonic building blocks. Exemplary devices that include such material include various optical devices, photonic space-time crystal generators, telecommunications, and anti-counterfeiting designs, among many others.

[0040] To differentiate the genuine time-crystalline order from a large variety of time-periodic patterns, stringent requirements have been introduced. First, these crystals should emerge from spontaneous time symmetry breaking, where the relative time phases are randomly distributed between 0 and 2π, assuring that the time crystals are independent of the external source. Second, time crystals should exhibit robustness against temporal perturbations by an external source, demonstrating a rigidity analogous to that of space crystals. Criteria-satisfying continuous time crystals have been reported for photonic metamaterials, optically pumped atomic system, Rydberg gases and electron-nuclear spin systems. However, continuous space-time crystals (CSTCs), which spontaneously break the time translation symmetry as well as the space translation symmetry without assistance of periodic driving, have not been convincingly demonstrated yet in either quantum or classical systems. Moreover, since most of the time crystals known so far exist in the quantum world, a time crystal has not been directly seen by microscopic observations or even with bare human eyes, at the same time being shown to meet the above identification criteria. While time-varying patterns can often be observed by naked eyes, they are typically not arising from many-body interactions of quasi-atom building blocks, and whether some of them could happen to meet the stringent requirements of being identified as time crystals remains an open question.

[0041] In accordance with examples described herein, classical CSTCs in nematic LC systems with emergent topological soliton exhibit interactions mediated by orientational elasticity. By shining (e.g., ambient) or microscope illumination light on specially designed samples with LC confined between glass plates coated by photo-responsive dye, we find emergent spatiotemporal patterns in which spatial and temporal symmetries are broken, without the assistance of periodic external driving. Furthermore, such emergent behavior can be directly observed in an optical microscope or other device and, when designed appropriately, even by bare eyes. The continuous space-time crystallization phase is quite

stable at room temperature and can persist locally for hours of our observation. By building a model based on balancing optical, surface and bulk viscoelastic torques associated with nematic fluid's orientational viscoelasticity, the emergent formation of topological solitons in this system can be explained. Periodically-varying configurations with elastically interacting spatially-localized particle-like topological solitonic structures can be constructed. We find that the intrinsic temporal periodic nature persists with changes of temperature and external driving light intensity, yielding good agreements with the experimental observations. Experimental and numerical verification that the time translation symmetry is broken spontaneously and the continuous space-time crystallization phase is robust against spatiotemporal dislocations and temporal perturbations, meeting all requirements to be identified as time-crystalline, are also observed. Various exemplary devices, such as optical devices, photonic space-time crystal generators, telecommunications, anti-counterfeiting designs, and cryptography, among many others, which use such material are described in more detail below in connection with FIG. 15.

[0042] Specific Examples

[0043] The specific examples are provided to illustrate the respective embodiments. Unless otherwise noted, the claims are not limited to the specific examples.

[0044] Emergence of the time-crystalline order

[0045] The samples are prepared by sandwiching the nematic liquid crystal (LC) with photo-responsive confining substrates, inner surfaces of which are coated with dye, as described herein. The photo-responsive (e.g., azobenzene dye) molecules at the surfaces and LC molecules in the bulk have anisotropic shapes, with their average orientations characterized by nonpolar directors $\mathbf{n}_s$ and $\mathbf{n}$ with head-tail symmetry ($\mathbf{n}_s \equiv -\mathbf{n}_s$ and $\mathbf{n} \equiv -\mathbf{n}$), respectively. When normally incident linearly polarized blue light passes through the samples (FIG. 1 (a)), $\mathbf{n}_s$ at the top surface tends to orient perpendicularly to the polarization direction of the linearly polarized light, and the LC molecules near it orient parallel to the azobenzene molecules, thus following the dye-defined surface boundary conditions (FIG. 1 (b)-(d)). For a monodomain LC and polarization direction of the linearly polarized light orthogonal to directors $\mathbf{n}_s$ at both top and bottom surfaces and $\mathbf{n}$ in the bulk, the light could traverse the sample as an ordinary mode without polarization change. However, the initial surface boundary conditions are tangentially degenerate. Upon the illumination of linearly polarized light, the dye molecules at the top surface become uniformly oriented along the direction

perpendicular to the polarization of incident light, whereas orientations of the dye molecules at the bottom substrate depend on their initial random polydomain orientations. Orientational changes of the LC director develop across the sample thickness, leading to transformation of the polarization state of the traversing light to generally elliptical polarization, as well as rotation of the long axis of polarization ellipse. Subsequently, as the bottom substrate is exposed to the elliptically polarized light, this leads to the reorientation of neighbouring LC molecules and $\mathbf{n}_s$ at the bottom surface, which tend to orient perpendicular to the major axis of the polarization ellipse of elliptically polarized light (FIG. 1 (d)). Once the dye molecules and $\mathbf{n}_s$ rotate, they also drive reorientations of the neighbouring LC molecules and $\mathbf{n}$, further changing the polarization ellipse of traversing polarized light. Such feedback mechanism spontaneously creates periodic spatiotemporal array of topological solitonic quasiparticles (FIG. 1 (e)), forming a robust continuous space-time crystallization phase (FIG. 1 (f) and FIG. 7), which will be described in detail below.

[0046] With the help of the first-order full-wave retardation plate (FIG. 1 (a)), the different orientations of the LC director in the bulk are inferred from polarized interference colors seen in the captured polarizing optical micrographs. For a thin cell (e.g., thickness d<2 μm), the light after the analyzer becomes blueish or yellowish (FIG. 1 (e)) when the director orientations are parallel or perpendicular to the slow axis of the retardation plate, respectively. The spatial area of an CSTC can be made larger than 1 mm^2, which can be observed directly by eyes and can be characterized in detail with an optical microscope. By selecting a fixed stripe area (dashed rectangle in FIG. 1 (e)) and tracking it in time, a space-time image of the solitonic arrays is composed, where the size of a representative time crystal region shown in FIG. 1 (f) is 400 μm·120 s. We analyze the normalized digital intensity signals (Φ) of pixels in FIG. 1 (f) and perform the Fast Fourier Transform analysis (FIG. 1 (g),(h)), showing a sharp peak at around 0.217 Hz (4.61 s), which corresponds to the temporal periodicity of the CSTC. By defining time correlation function $G(t) = \langle\Phi(t)\Phi(0)\rangle - \langle\Phi(t)\rangle\langle\Phi(0)\rangle$ from the normalized digital intensity signals within the pattern , we find that $G(t)$ can be fitted by a power-law decay ($\sim t^{-0.09}$) despite fluctuations, exhibiting a quasi-long-range order in time (FIG. 8), similar to that known for systems with one-dimensional spatial positional order like smectic LCs that follow the Peierls and Landau's predictions.

[0047] Numerical modeling of emergent particle-like solitonic structures and crystals

[0048] To gain insights into the emergent formation of particle-like topological solitons that then exhibit time crystallization, we use a model based on the balance of optical, surface anchoring and bulk viscous and elastic torques, with the latter derived from the Frank-Oseen free energy:

$$F_{\text{bulk}} = \int \mathrm{d}^3\boldsymbol{r}\left\{\frac{K_{11}}{2}(\nabla\cdot\boldsymbol{n})^2 + \frac{K_{22}}{2}[\boldsymbol{n}\cdot(\nabla\times\boldsymbol{n})]^2 + \frac{K_{33}}{2}[\boldsymbol{n}\times(\nabla\times\boldsymbol{n})]^2\right\}, \quad (1)$$

[0049] where the Frank elastic constants K_{11}, K_{22}, and K_{33} depend on temperature and determine energetic costs of, respectively, splay, twist and bend spatial deformations of the LC director field, **n**(**r**). Furthermore, the free energy term associated with coupling **n**(**r**) and $\mathbf{n}_s$(**r**) at surfaces reads

[0050] $$F_{\text{surface}} = -\int \mathrm{d}^2\boldsymbol{r}\,\frac{\eta W}{2}(\boldsymbol{n}_s\cdot\boldsymbol{n})^2, \quad (2)$$

where η is the dimensionless light coupling efficiency parameter ranging from 0 to 1 and W is the anchoring coefficient. We assume that $\mathbf{n}_s$ orients perpendicular to the direction of major axis of the elliptically polarized light, calculated using the Jones-matrix method. While our field theory model is intended to describe spatial structures of the director field, solitonic topological particles emerge spontaneously within it, much like skyrmions, domain walls and hopfions found in diverse fields ranging from magnets to LCs. In turn, these particle-like solitonic objects then exhibit many-body interactions and the time-crystalline order.

[0051] Consider a uniform state of director field with a small perturbation on the left side (FIG. 9), when light (450 nm) normally incident on the sample from the top has linear polarization along y axis. The resulting director dynamics stems from the torque balance

$$\frac{\delta F}{\delta \boldsymbol{n}_i} = -\gamma\frac{\partial \boldsymbol{n}_i}{\partial t}$$

yielding the temporal evolution $\mathbf{n}_i$(t), where

$$\frac{\delta F}{\delta \boldsymbol{n}_i}$$

is the variational derivative of F, subscript i denotes spatial coordinates, γ is the rotational viscosity, Jones vectors are updated further in each next iteration and $F=F_{bulk}+F_{surface}$. A spatially periodic configuration of the solitonic array emerges spontaneously (FIG. 2 and FIG. 9). By properly arranging the initial state for periodic boundary conditions, such as described herein, one finds that the simulated structure shown in FIG. 2 (a) exhibits properties of a continuous space-time crystal phase.

[0052] In the dynamic steady-state configuration, the director field $\mathbf{n}(\mathbf{r})$ at the top surface stays perpendicular to the incident light's polarization direction and smoothly deforms at the bottom (FIG. 2 (a)), displaying alternating pairs of the nematic Néel domain wall solitons of opposite elementary topological charge (FIG. 2 (a),(b)). These solitons are labelled as the elements of the first homotopy group $\pi_1(\mathbb{S}^1/\mathbb{Z}_2)\equiv\pi_1(\mathbb{S}^1)=\mathbb{Z}$ and can be treated as topological quasiparticles of opposite signs ±1, low-dimensional analogues of Skyrme solitons used to model particles with different baryon numbers in subatomic physics. Treating the time coordinate similarly to the space coordinates, ±1 elementary quasiparticle-like topological solitons can also be identified in time. By calculating the elastic free energy of the LC director field deformations above the solitonic walls in the dye orientations and the adjacent LC director field (FIG. 2 (a)-(c)), one finds that elasticity-mediated interactions between the solitonic quasiparticles can be equivalently represented with the help of topological elastic bonds connecting the neighbouring interacting quasiparticles (FIG. 2 (d)), forming a many-body interaction system. Because the entire system is topologically neutral (no net topological charge), individual quasiparticles cannot be smoothly eliminated but rather only can vanish through annihilating pairs of them, which would require a large energetic barrier. By analysing the relative displacements distribution of neighbouring +1 Néel domain wall solitons associated with different spatial lattices at different times in the space-time crystal, we find that the relative displacements follow a Gaussian distribution (FIG. 2 (e)), corresponding to an effective harmonic potential energy landscape (FIG. 2 (f)) under small thermally driven displacements. Such an energy landscape describing the quasiparticle interactions resembles that found in a colloidal particle crystal system in liquid crystal media, where the energy differences are several kBTem corresponding to ~10% displacements (k_B is the Boltzmann constant and T_{em} is the temperature). This indicates that, albeit all emergent from and describable by the field theory of the LC director field, many-body interactions between the quasiparticles maintain the order of space-time crystals.

[0053] The close agreements between computer-simulated and experimental polarizing optical micrographs (FIG. 1 (e), FIG. 2 (g) and FIG. 10 (a),(b)) and three-photon excitation fluorescence polarizing microscopy images (FIG. 10 (c),(d)) validate our analysis of CSTC configurations. Similarly, the theory-experiment agreements of space-time polarizing optical micrographs and videos support the reconstructed configuration of the CSTC (FIG. 1 (f) and FIG. 2 (h)).

[0054] Diversity and control of the space-time periodic structures

[0055] In addition to the emergence of time-space-periodic domain wall arrays, by superimposing the light patterns from two CSTCs, we find that the overlapping spatial solitonic arrays can allow us to form orthorhombic and monoclinic lattices. The corresponding combined space-time patterns exhibit the same space-time lattices (FIG. 11). Due to the non-equivalence between spatial and temporal coordinates, we only find the 1+1 dimensional (1 + 1D) space-time orthorhombic and monoclinic lattices (intrinsically different from the 2D wallpaper space groups), consistent with previous theoretical proposals. This result reveals the possibility of achieving a richer space-time group structure in higher dimensions, as obtained here by incorporating the time coordinate into the spatial symmetry group.

[0056] External stimuli allow for controlling the studied emergent spatiotemporal order. The temporal periodicity of CSTC increases as the driving light intensity decreases (FIG. 2 (i), FIG. 12). Below a certain threshold (~1 mW cm^{-2}), the continuous space-time crystallization phase transforms to a time-symmetry-unbroken (TSU) phase, where the LC director field becomes static. Computer simulations qualitatively reproduce this behavior as the temporal periodicity decreases with increasing η (FIG. 2 (j)), and the structure eventually relaxes to the spatially uniform planar state (FIG. 13) at efficiencies below a certain threshold (η~0.3). The temporal periodicity also decreases with increasing temperature, until the system reaches a disorder phase (FIG. 2 (i), (j)). Noteworthily, the Frank elastic constants and birefringence of the LCs decrease by more than 30% within such a temperature change, indicating a good robustness of the CSTCs that can withstand changes of these material parameters. Experimental observations with changing temperature and driving light intensity in the same sample are consistent with computer simulations that yield spatial periodicity relatively insensitive to temperature and light coupling efficiency. For different LC cells with high birefringence and varying thickness, the temporal periodicities can be controlled to range from tens of seconds to milliseconds. Second-scale time crystals could be employed for

interfacing with biological and organic holographic materials, which, in turn, can be potentially used for optical signal amplification, data storage, and phase conjugation.

[0057] Testing against stringent criteria for time-crystalline identification

[0058] Meeting a key criterium of time crystallinity, our space-time crystals exhibit good robustness against spatial and temporal perturbations (FIG. 3). The CSTCs are found to recover defect-free order within tens of temporal periods after an emergence of space-time dislocation (FIG. 3 (a)). Interestingly, by reconstructing the space-time coordinates, we find that the profiles after the dislocation emergence can be fitted by the nonlinear theory of an edge dislocation in smectic crystal systems (FIG. 3 (b)), showing similarity of spatial and temporal quasi-particle displacements resembling that of molecules in smectics in higher dimensions. The space-time crystals are also stable under temporal perturbations, to confirm the robustness against temporal perturbations (FIG. 3 (c)-(i)), we use blue light with temporally randomized intensity (randomly distributed within the range $[\alpha,1]W_{driving}$, where α is the parameter controlling the strength of perturbation and $W_{driving}$ is the maximum driving light intensity) to illuminate the sample and red light in a separate channel for imaging, the continuous space-time crystallization order persists well under small temporal perturbations of incident light intensity (α = 0.8 and $W_{driving}$ = 1.5 $mWcm^{-2}$). The effect of temporal perturbations can be quantified by measuring the crystalline fraction parameter, Ξ. Both experiments and computer simulations show that the crystalline fraction does not change much when the perturbation is within a certain range (FIG. 3 (f)-(i)), which corresponds to the space-time crystal phase. As α decreases, the perturbation becomes larger and Ξ suddenly drops, because the system experiences a phase transition and becomes disordered (FIG. 3 (g),(i)).

[0059] As anticipated for space-time crystals, the continuous time translation symmetry of CSTCs is spontaneously broken independently of the driving light source. To reveal this, we repeatedly measure the time phase each time after blocking and shining the blue light to a CSTC area (FIG. 4 (a),(b)), finding the relative time phases randomly distributed between 0 and 2π (FIG. 4 (c)). By blocking and unblocking the external light source and tracking the director field (FIG. 4 (d),(e)) we also reproduce this general behavior in computer simulations that closely agree with experiments.

[0060] Comparison to other classical time-periodic effects

[0061] We have described the observation of classical CSTCs in nematic LCs, which emerge at room temperature and can be designed to be seen by optical microscopes or even directly by human eyes. These spatiotemporal states usually emerge within an area (FIGS. 9 and 14) where the one-dimensional spatial symmetry and temporal symmetry are spontaneously broken in a continuous manner, forming 1 + 1D CSTCs. This emergent behavior is different from the case of active (moving) crystals, where a pre-set crystal structure can spatially translate while periodically entering similar states of the spatially periodic lattice, driven by external electric signals. Breaking of temporal symmetry of these active crystals refers to the breaking of spatial translation symmetry, and the active lattice time periodicity depends on the collective moving speed of spatial crystallites, differently from our time crystals.

[0062] CSTCs persist locally for hours while the temporal periodicity changes only slightly (by ~10%) after ~1 hour of observations, where properties of LCs largely define their behavior. The emergent bonded quasiparticles reveal robustness against temporal and spatial perturbations, demonstrating intrinsic time crystallinity features and meeting identification criteria that so far have not been probed for other classical temporally periodic systems like chemical oscillators and dissipative structures (potential candidates for time crystallinity of physical behavior, which remain to be tested against the identification criteria). Our CSTCs are the first classical topological solitonic system that meets all time crystal's stringent requirements introduced so far.

[0063] While we focused on 1 + 1D CSTCs, by introducing higher dimensional topological solitons or defects and their arrays, 2 + 1D and 3 + 1D and other CSTCs can be observed.

[0064] Applications

[0065] CSTCs in highly technological LC materials can be used for various applications, such as in optical devices, photonic space-time crystal generators, and telecommunications. Since the spatial structures of CSTCs consist of the Néel domain wall solitons, when polarized light passes through the nematic LC slab with such topological solitons at one surface and periodic director deformations extending throughout the nematic bulk, the traversing polarized light accumulates phase retardation according to the director's spatially and temporally varying orientations (FIG. 5). This property may enable the fabrication of dynamic time-crystalline Pancharatnam-Berry phase (geometric phase) gratings and lenses (also

known as cycloidal diffractive waveplates). We note that the phase accumulations vary not only with spatial coordinates but also with temporal coordinates, where the outgoing light's polarization state depends on the wavelength and polarization of the input light (FIG. 5 (b)-(d)). Therefore, such LC-based space-time crystals can be used for generating photonic space-time crystals, assuming that the spatial periodicity can be reduced to approach the visible light's wavelengths and the temporal frequencies can be much higher. In addition, one can combine CSTC-modulated light with the driving light, allowing CSTCs to change the polarization states of the accompanying modulated light without affecting CSTC's 4D structures. For example, as the typical wavelength range used in fiber optical telecommunications (>850 nm) differs from that of the driving light (~450 nm) to which azobenzene dye is sensitive, optical signal modulation and information encoding at wavelengths outside the spectral range of the azobenzene dye's sensitivity could be implemented based on the CSTC's robust temporal and spatial order (FIG. 5 (c),(d)).

[0066] The ambient-intensity light-driven and non-contact properties of CSTCs make them suitable for anti-counterfeiting device with the protection at multiple implementation levels in which the temporal and spatial periodic structures can spontaneously emerge (FIG. 6 (a)-(c)). This "time watermark" can be fabricated at low cost, since a 1 cm × 1 cm × 2 μm sample requires only ~2 × 10-14 g of LC and the surface monolayer with <10-14 g of the azobenzene dye that can be sandwiched between glass or other surfaces. Due to the spontaneous temporal symmetry breaking, the time crystals can be exploited in pseudo-random number generators. By combining multiple CSTCs, the synthetic systems generate unique, fingerprint-like states corresponding to the spatiotemporal topological soliton arrays (FIG. 6 (d),(e)) each time they emerge, maintaining order for a remarkably long time (FIG. 8). Additionally, the phases of CSTCs can be tuned by smoothly switching the driving light intensity (FIG. 6 (f)), allowing for the creation of a 2 + 1D barcode via superimposing multiple CSTCs (FIG. 6 (g)). As the 2D barcode can store over 100 times more bits than a 1D barcode, the capacity of storing information with proper data coding in higher-dimensional barcodes like 2 + 1D is effectively unbounded due to the extra temporal coordinate (>100,000 bits per second). The intrinsic robustness of the space-time order, supported by the time-crystallinity of topological solitons, could further enhance error correction capabilities of 2 + 1D barcodes. For the third level of the anti-counterfeiting uses, the temporal periodicity of CSTCs can be utilized as keys in cryptographic systems. For example, with two CSTCs having temporal

periodicities T_1 and T_2 (assuming $T_1<T_2$), an identical spatial pattern only recurs after a time interval of $(T_1\times T_2)/(T_2-T_1)$ (FIG. 6 (h)), which could be used to check authenticity. CSTCs with different temporal periodicities can be introduced by incorporating pre-programmed light intensity filters. The entire system may display disorder-like spatiotemporal behavior, however, within each CSTC, the time-crystalline order with a specific temporal periodicity can be maintained for a long time. Overall, the entire fingerprint-like CSTC states can be precisely predicted if the information about the pre-programmed light intensity filters (the system's keys) is known (FIG. 6 (i)) and can be utilized for anti-counterfeiting purposes.

[0067] Exemplary Materials and sample preparation

[0068] The glass substrates were coated with photo-responsive material 2-(4-dimethylamino-phenylazo)-N-(3-triethoxysilane-propyl)-benzamide (dMR)[35,61], which is sensitive to the blue and violet light and insensitive to the red light. To coat monolayer dMR on the glass surfaces, we submerge the glass plates into a 1 wt% solution of dMR in toluene at a temperature of 45 °C. After a 90-min submersion, the dMR molecules are bonded to the glass surfaces; we then wash away the excess dMR by a toluene rinse, followed by blowing the glass plates with dry nitrogen and curing them at 115 °C for 2 hours. The LC cells are constructed using two glass substrates coated with monolayers of dMR, where the cell thickness d = 2-4 μm is defined by glass spheres mixed with a methanol-diluted epoxy. Once the epoxy has cured, we fill the cell via capillary forces with nematic 4-cyano-4'-pentylbiphenyl (5CB, EM Chemicals).

[0069] Quasi-long-range order and relative time phases of the CSTC

[0070] To obtain the time order of CSTCs, we calculate the correlation function G in time coordinate, which is a common tool for analyzing the spatial order of crystals and liquid crystals. For crystals, the spatial correlation function $G(r)$ is a constant, where r is the distance between the two measured positions. For smectic liquid crystals, the spatial correlation function $G(r)$ decays as $\sim r^{-\zeta}$ ($\zeta<0.15$) along the smectic layers, which is a quasi-long-range order[37]. For CSTCs, we measure the normalized digital signal $\Phi_i(t)$ of each pixel at different times, where subscript i denotes spatial coordinates. The correlation function $G(t)= \sum_i G_i(t)= \sum_i\langle\Phi_i(t)\Phi_i(0)\rangle-\langle\Phi_i(t)\rangle\langle\Phi_i(0)\rangle$ is calculated with 2200 spatial pixels and 9000 temporal frames, showing a quasi-long-range order in time.

[0071] In experiment, the relative time phases are measured from 100 experimental realizations. In each realization, the driving light is blocked with red colour filter at first

(allowing only red color light to pass through). Subsequently, we remove the red color filter, and the CSTC spontaneously emerges. After a time interval Δt (Δt = 60s), we start measuring the light signals from the recorded video, and calculate the phase using Fast Fourier Transform analysis function in MATLAB (MathWorks).

[0072] FIG. 15 illustrates a device 1500 in accordance with examples of the disclosure. Device 1500 can be the same or similar to the device illustrated in FIG. 1 (a). Device 1500 includes a first substrate 1502, a second substrate 1504, one or more photo-responsive dye layers 1508, 1510, and a nematic liquid crystal material 1506 between first substrate 1502 and second substrate 1504. Device 1500 is configured, such that in response to an applied light, a continuous space-time crystallization phase forms within the nematic liquid crystal material. In accordance with examples of the disclosure, the nematic liquid crystal material comprises one or more of 5CB(4-Cyano-4'-pentylbiphenyl) or E7 (a mixture of 4-Cyano-4'-pentylbiphenyl, 4'-Heptyl-4-biphenylcarbonitrile, 4'-Octyloxy-4-biphenylcarbonitrile and 4-Cyano-4'-Pentylterphenyl). In accordance with further examples, photo-responsive dye layer(s) 1508, 1510 are coated onto an inner surface of one or more of first substrate 1502 or second substrate 1504. In accordance with further examples, the photo-responsive dye layer comprises an azo compound. For example, the photo-responsive dye layer can be or include azobenzene or 2-(4-dimethylamino-phenylazo)-N-(3-triethoxysilane-propyl)-benzamide (dMR). In some cases, the light comprises ambient light. In some cases, device 1500 can include a light source 1512. Light source 1512 can be a polarized light source source proximate the first substrate. In some cases, device 1500 can include a polarizer 1514 to polarize light from light source 1512 or ambient light.

[0073] As described above, device 1500 can exhibit 1 + 1D continuous space-time crystal behavior, 0 + 1D continuous space-time crystal behavior, 2 + 1D continuous space-time crystal behavior, or 3 + 1D continuous space-time crystal behavior. In accordance with further examples, an output of light from the device is dependent on the wavelength(s) and polarization of an input light to the device. In some cases, the nematic liquid crystal material includes anisotropic particles 1510 therein. Exemplary anisotropic particles include 4-Cyano-4'-pentylbiphenyl having a first dimension of between about 0.1 and 10 nm or about 0.5 nm and a second dimension of between about 0.5 and 5 nm or about 2 nm. In some cases, the second dimension is at least about 3 to about 10 times greater than the first dimension.

[0074] In accordance with further examples, device 1500 forms part of a telecommunications device, cryptography device, optical device, photonic time crystal generator, anti-counterfeiting system, or barcode device, or the like.

[0075] The example embodiments of the disclosure described herein do not limit the scope of the invention, since these embodiments are merely examples of the embodiments of the invention. Any equivalent embodiments are intended to be within the scope of this invention. Indeed, various modifications of the disclosure, in addition to the embodiments shown and described herein, such as alternative useful combinations of the elements described, may become apparent to those skilled in the art from the description. Such modifications and embodiments are also intended to fall within the scope of the appended claims.

CLAIMS:

1. A device comprising:

a first substrate;

a second substrate;

a photo-responsive dye layer; and

a nematic liquid crystal material between the first substrate and the second substrate,

wherein, in response to an applied light, a continuous space-time crystallization phase forms within the nematic liquid crystal material.

2. The device of claim 1, wherein the nematic liquid crystal material comprises one or more of 5CB(4-Cyano-4'-pentylbiphenyl) or E7 (a mixture of 4-Cyano-4'-pentylbiphenyl, 4'-Heptyl-4-biphenylcarbonitrile, 4'-Octyloxy-4-biphenylcarbonitrile and 4-Cyano-4'-Pentylterphenyl).

3. The device of claim 1, wherein the photo-responsive dye layer is coated onto an inner surface of one or more of the first substrate or the second substrate.

4. The device of claim 1, wherein the photo-responsive dye layer comprises an azo compound.

5. The device of claim 4, wherein the photo-responsive dye layer comprises azobenzene or 2-(4-dimethylamino-phenylazo)-N-(3-triethoxysilane-propyl)-benzamide (dMR).

6. The device of claim 1, wherein the light comprises ambient light.

7. The device of claim 1, wherein the light is from a light source.

8. The device of claim 1, further comprising a polarized light source proximate the first substrate.

9. The device of claim 1, wherein the device exhibits 1 + 1D continuous space-time crystal behavior.

10. The device of claim 1, wherein the device exhibits 0 + 1D continuous space-time crystal behavior.

11. The device of claim 1, wherein the device exhibits 2 + 1D continuous space-time crystal behavior.

12. The device of claim 1, wherein the device exhibits 3 + 1D continuous space-time crystal behavior.

13. The device of claim 1, wherein the output of light from the device is dependent on the wavelength(s) and polarization of an input light to the device.

14. A continuous space-time crystal device comprising:

a first substrate;

a second substrate;

a nematic liquid crystal material between the first substrate and the second substrate, the nematic liquid crystal material comprising anisotropic particles; and

a photo-responsive dye layer coated onto one or more of the first substrate and the second substrate.

15. The device of claim 14, wherein the device exhibits 1 + 1D continuous space-time crystal behavior.

16. The device of claim 14, wherein the device exhibits 0 + 1D continuous space-time crystal behavior.

17. A telecommunications device comprising the device of any of claims 1-16.

18. A cryptography device comprising the device of any of claims 1-16.

19. An optical device comprising the device of any of claims 1-16.

20. A photonic time crystal generator comprising the device of any of claims 1-16.

21. An anti-counterfeiting system comprising the device of any of claims 1-16.

22. A barcode device comprising the device of any of claims 1-16.

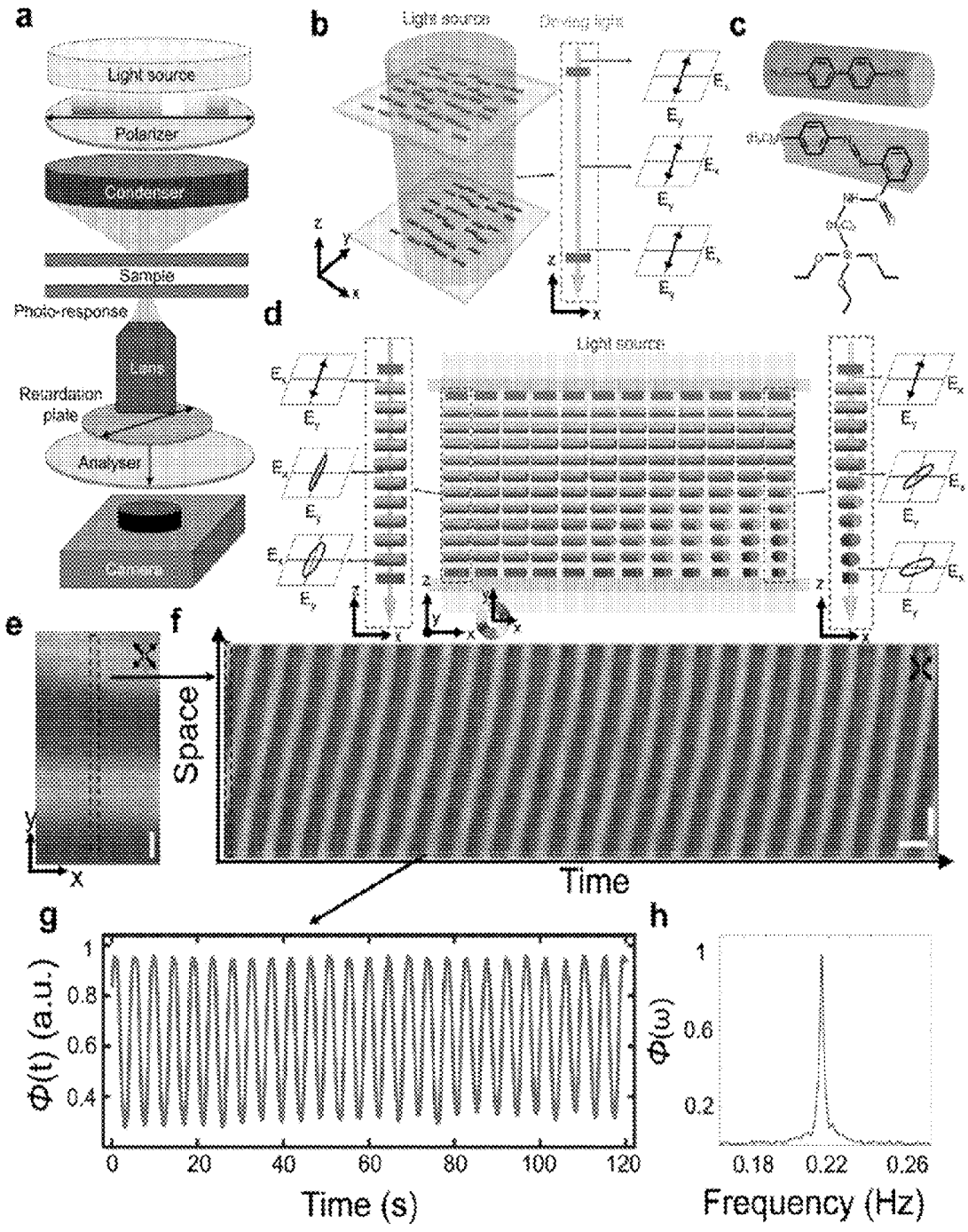
a
Light source
Polarizer
Condenser
Sample
Photo-response
Lens
Retardation plate
Analyser
Detector
b
Light source
Driving light
c
d
Light source
e
f
Space
Time
g
Φ(t) (a.u.)
Time (s)
h
Φ(ω)
Frequency (Hz)

FIG. 1

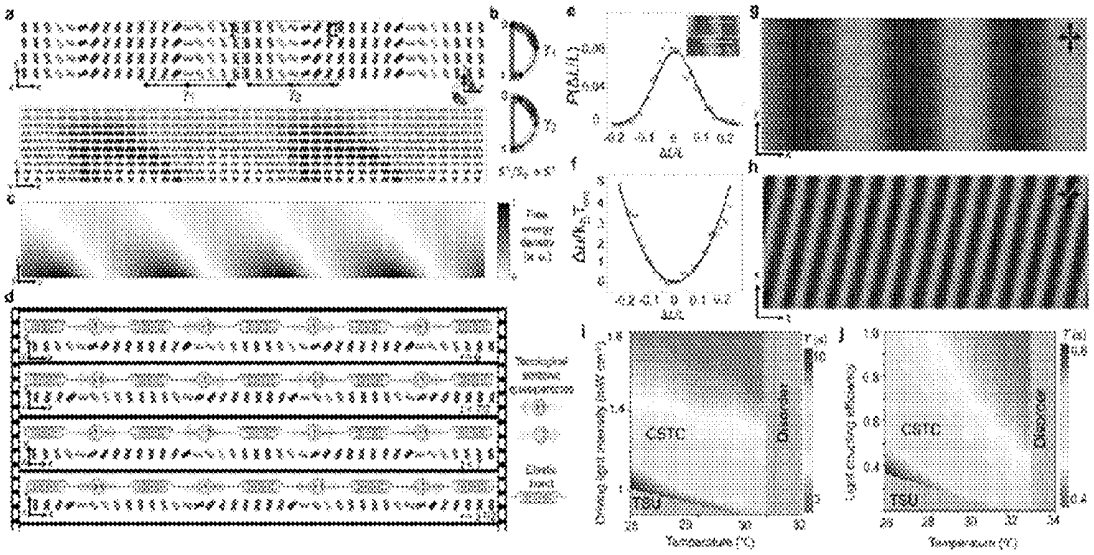
CSTC
TSU
Decoupling
Temperature (°C)

FIG. 2

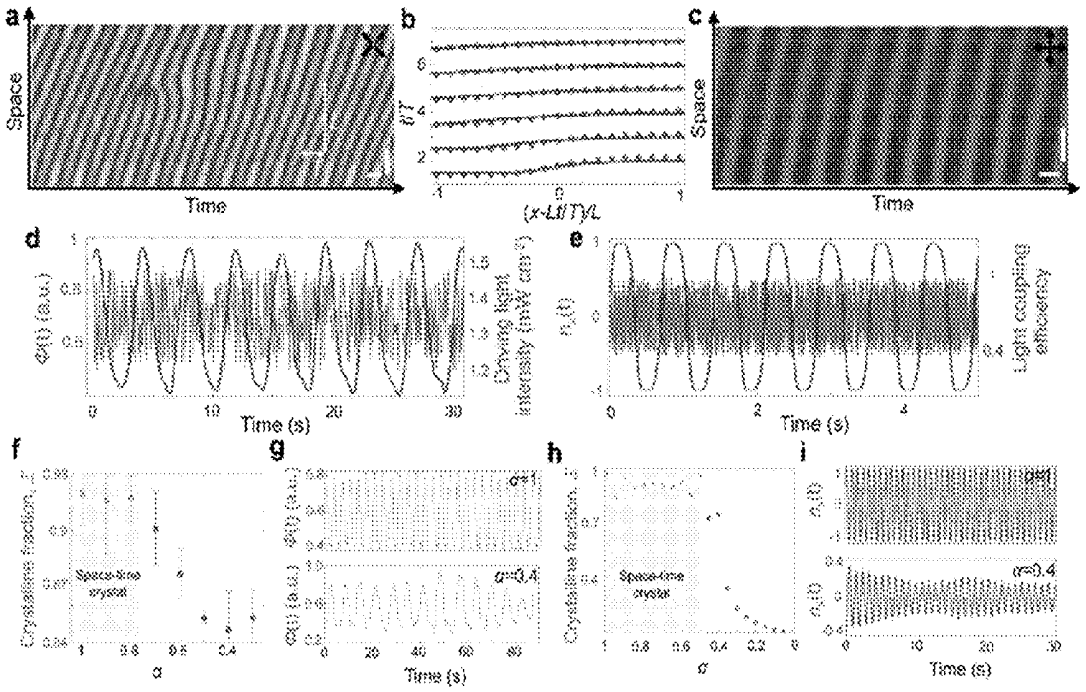
Space
Time
Time (s)
Light coupling efficiency
Crystalline fraction
Space-time crystal

FIG. 3

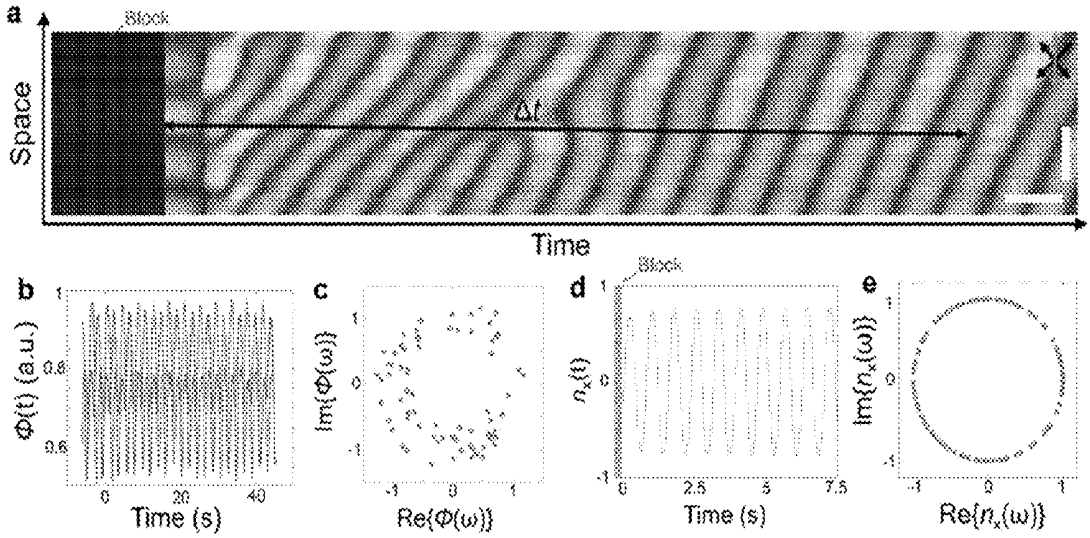
a
Stock
Space
Δt
Time
b
Φ(t) (a.u.)
Time (s)
c
Im{Φ(ω)}
Re{Φ(ω)}
d
Stock
$n_x(t)$
Time (s)
e
Im{$n_x(\omega)$}
Re{$n_x(\omega)$}

FIG. 4

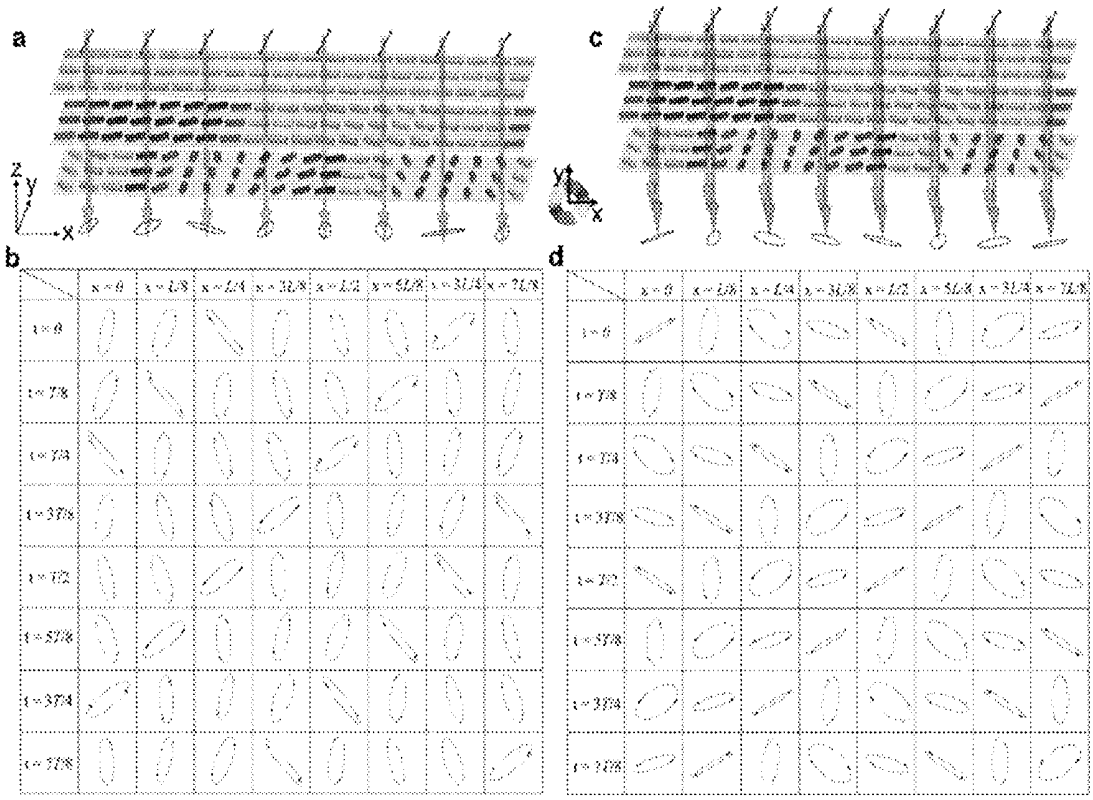

FIG. 5

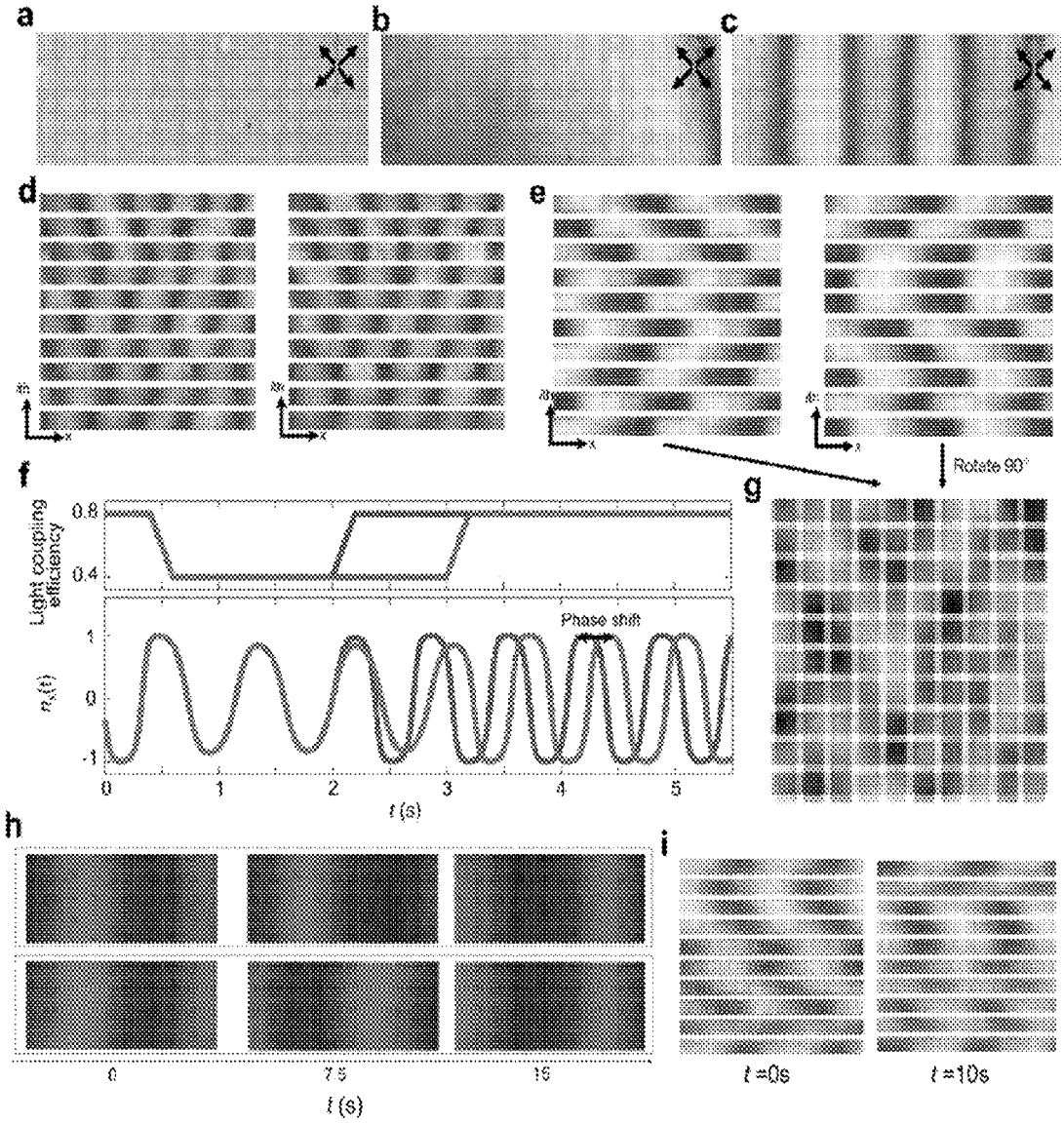
a
b
c
d
e
Rotate 90°
f
g
Light coupling efficiency
0.8
0.4
Phase shift
1
0
-1
0
1
2
3
4
5
t (s)
h
i
0
7.5
15
t (s)
t =0s
t =10s

FIG. 6

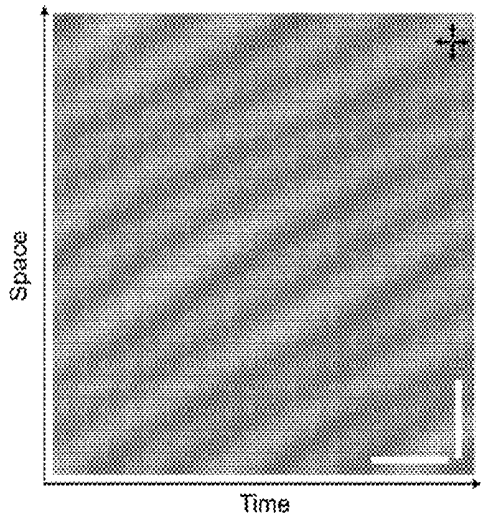

FIG. 7

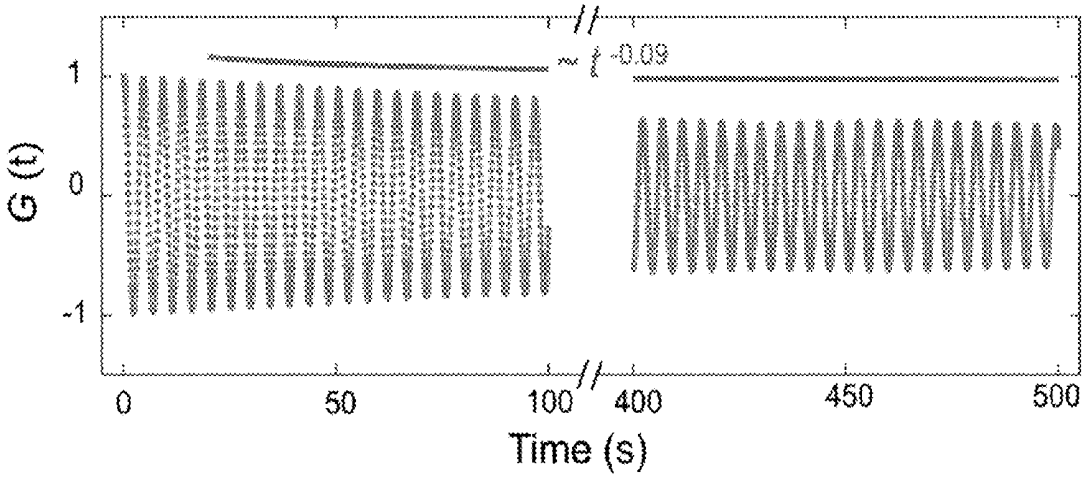

FIG. 8

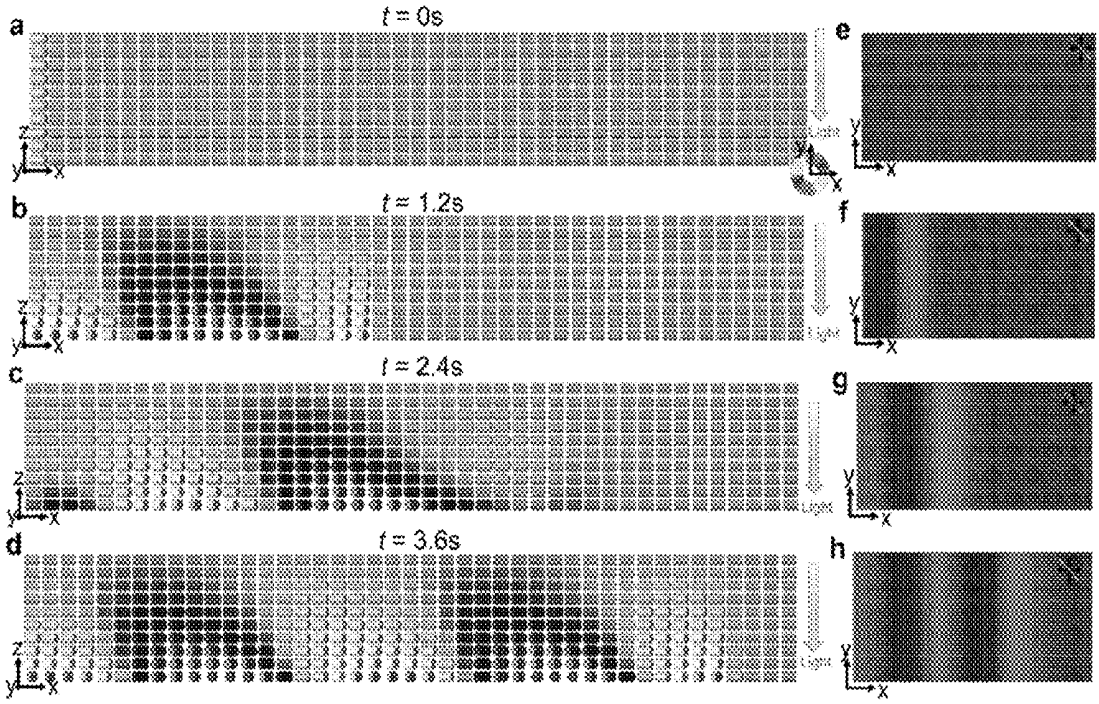

FIG. 9

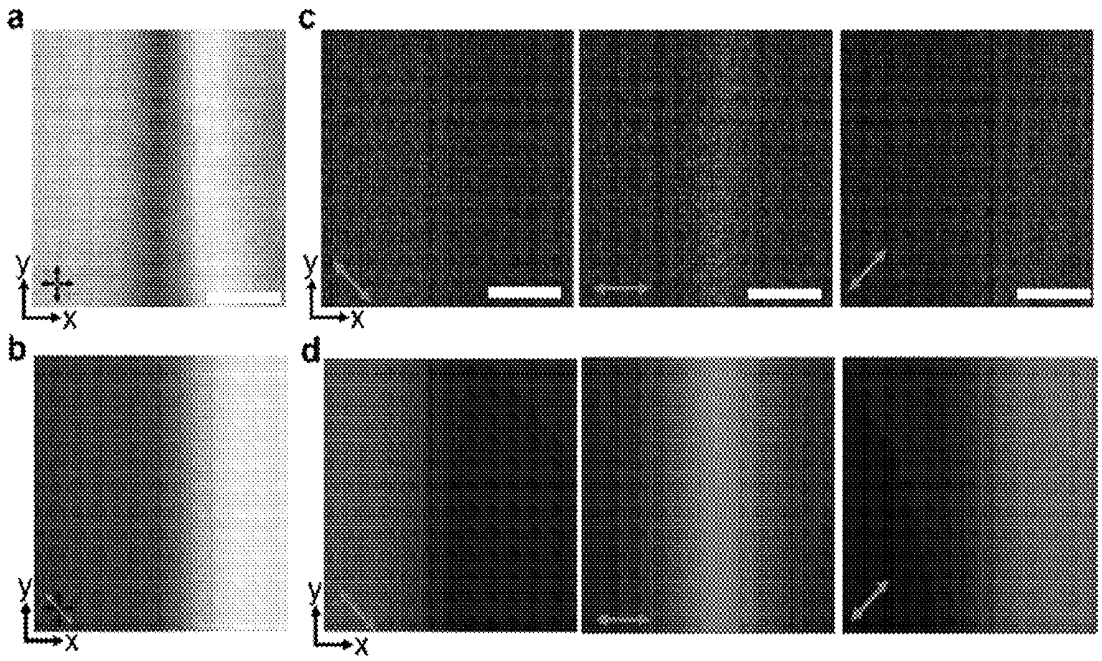

FIG. 10

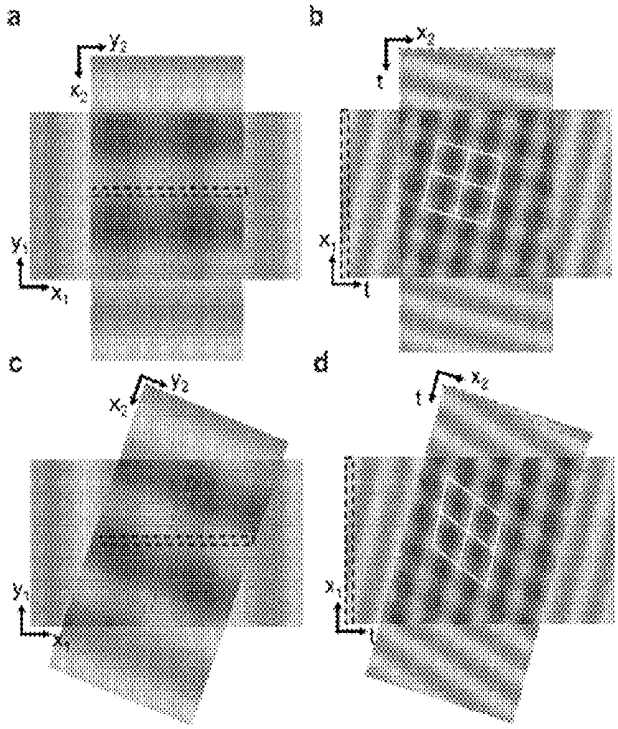

FIG. 11

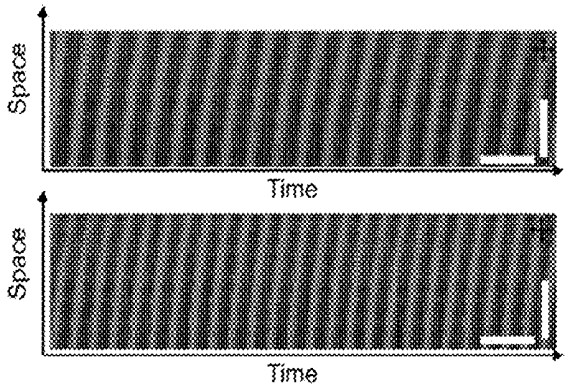

FIG. 12

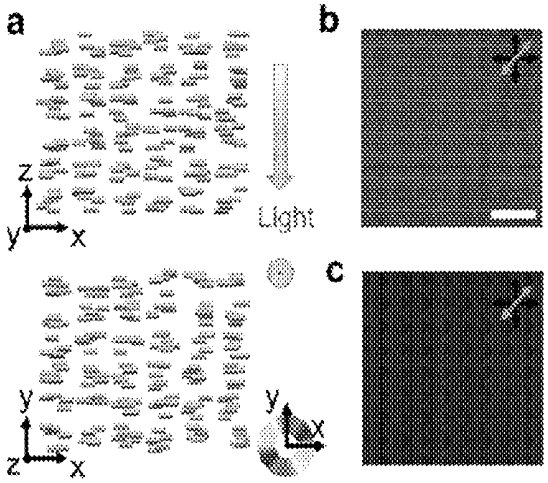

FIG. 13

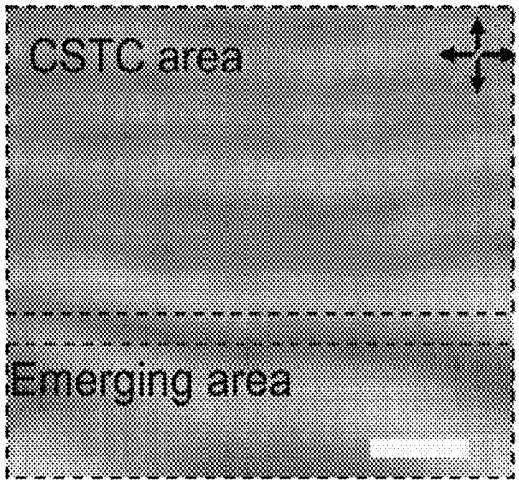

FIG. 14

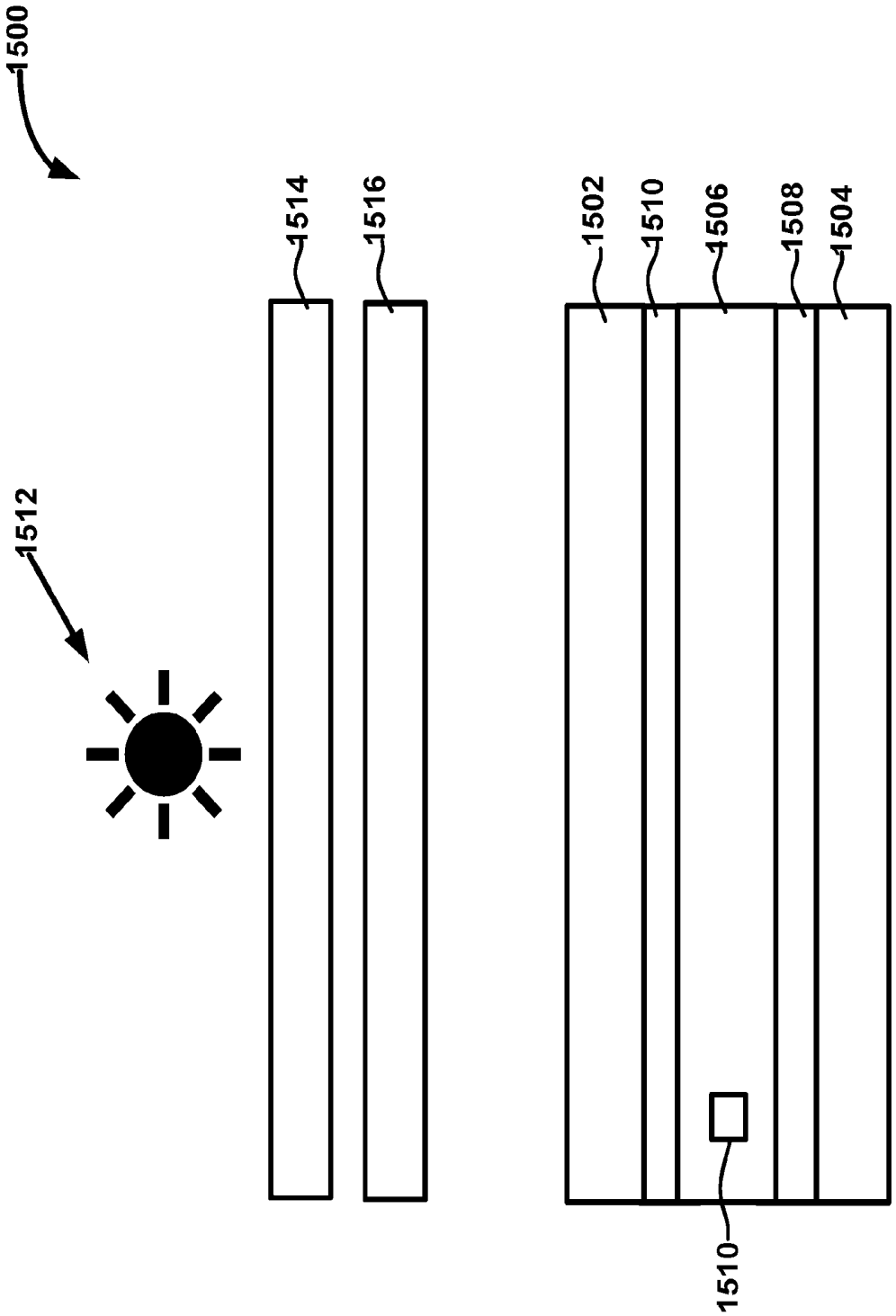

FIG. 15

INTERNATIONAL SEARCH REPORT

International application No.
PCT/US2026/017119

A. CLASSIFICATION OF SUBJECT MATTER

IPC: ***G02F 1/139*** (2026.01); ***G02B 5/30*** (2026.01); ***G02F 1/1334*** (2026.01); *C08J 3/28* (2026.01); *C09K 19/52* (2026.01)

CPC: ***G02F1/139; G02B5/30; G02F1/1334;*** *C08J3/28; C09K19/52*

According to International Patent Classification (IPC) or to both national classification and IPC

B. FIELDS SEARCHED

Minimum documentation searched (classification system followed by classification symbols)

See Search History Document

Documentation searched other than minimum documentation to the extent that such documents are included in the fields searched

See Search History Document

Electronic data base consulted during the international search (name of data base and, where practicable, search terms used)

See Search History Document

C. DOCUMENTS CONSIDERED TO BE RELEVANT

Category*	Citation of document, with indication, where appropriate, of the relevant passages	Relevant to claim No.
Y	US 2017/0309215 A1 (SAMSUNG ELECTRONICS CO., LTD.) 26 October 2017 (26.10.2017) Paragraphs [0066], [0085], [0193]	6, 17, 18/6, 19, 20/6, 21/6, 22
Y	US 2024/0402557 A1 (THE REGENTS OF THE UNIVERSITY OF COLORADO, A BODY CORPORATE) 05 December 2024 (05.12.2024) Paragraph [0027]	13, 17-22/13
Y	US 2014/0268332 A1 (THE REGENTS OF THE UNIVERISTY OF MICHIGAN) 18 September 2014 (18.09.2014) Paragraph [0084]	18, 21
Y	WO 2011/012890 A1 (CAMBRIDGE ENTPRISE LIMITED) 03 February 2011 (03.02.2011) Page 9, Paragraphs [2]-[4]	20

☑ Further documents are listed in the continuation of Box C. ☐ See patent family annex.

* Special categories of cited documents:
"A" document defining the general state of the art which is not considered to be of particular relevance
"D" document cited by the applicant in the international application
"E" earlier application or patent but published on or after the international filing date
"L" document which may throw doubts on priority claim(s) or which is cited to establish the publication date of another citation or other special reason (as specified)
"O" document referring to an oral disclosure, use, exhibition or other means
"P" document published prior to the international filing date but later than the priority date claimed
"T" later document published after the international filing date or priority date and not in conflict with the application but cited to understand the principle or theory underlying the invention
"X" document of particular relevance; the claimed invention cannot be considered novel or cannot be considered to involve an inventive step when the document is taken alone
"Y" document of particular relevance; the claimed invention cannot be considered to involve an inventive step when the document is combined with one or more other such documents, such combination being obvious to a person skilled in the art
"&" document member of the same patent family

Date of the actual completion of the international search	Date of mailing of the international search report
05 May 2026 (05.05.2026)	**27 May 2026 (27.05.2026)**

Name and mailing address of the ISA/US	Authorized officer
COMMISSIONER FOR PATENTS **MAIL STOP PCT, ATTN: ISA/US** **P.O. Box 1450** **Alexandria, VA 22313-1450** **UNITED STATES OF AMERICA**	**SHANE THOMAS**
Facsimile No. **571-273-8300**	Telephone No. **PCT Helpdesk: (571) 272-4300**

C. DOCUMENTS CONSIDERED TO BE RELEVANT

Category*	Citation of document, with indication, where appropriate, of the relevant passages	Relevant to claim No.
Y	Amaral et al. "Liquid crystal torons in Poiseuille-like flows" Nature Portfolio; Article [online]. 21 January 2025 [retrieved 05 May 2026]. Retrieved from the Internet: https://www.nature.com/articles/s41598-024-83294-7 Introduction, Toron elongation, Methods, Figure 1, pages 1, 3, 7	1-22
Y	Kundu et al. "In situ homeotropic alignment of nematic liquid crystals based on photoisomerization of azo-dye, physical adsorption of aggregates, and consequent topographical modification" Advanced Materials; Article [online]. 13 May 2013 [retrieved 05 May 2026]. retrieved from the Internet: https://pubmed.ncbi.nlm.nih.gov/23666876/ Pages 3365-3367, 3370	1-22
Y	Xu et al. "Space-time crystal and space-time group" Physical review Letters; Article [online]. 27 February 2018 [retrieved 05 May 2026]. retrieved from the Internet: https://link.aps.org/accepted/10.1103/PhysRevLett.120.096401 Introduction, page 1	9-12, 15-16, 17-22/ (9-12 and 15-16)
P,X	Zhao et al. "Space-time crystals from particle-like topological solitons" Nature Materials; Article [online]. 4 September 2025 [retrieved 4 May 2026]. Retrieved from the Internet: https://www.nature.com/articles/s41563-025-02344-1 Entire Document	1-22